Letter

Self-energy corrections to zone-edge acoustic phonons in monolayer and bilayer WS_2

Qixing Wang,[1] Yu Li Huang,[2] Qi Zhang,[3] Jiayu Ma,[4] Xin Luo,[4,*] and Yun-Mei Li[1,†]

[1]*Department of Physics, College of Physical Science and Technology, Xiamen University, Xiamen 361005, China*

[2]*Joint School of National University of Singapore and Tianjin University, International Joint Institute of Tianjin University, Fuzhou 350207, China*

[3]*School of Physics and Key Laboratory of MEMS of the Ministry of Education, Southeast University, Nanjing 211189, China*

[4]*State Key Laboratory of Optoelectronic Materials and Technologies, Guangdong Provincial Key Laboratory of Magnetoelectric Physics and Devices, Centre for Physical Mechanics and Biophysics, School of Physics, Sun Yat-sen University, Guangzhou 510275, China*

(Received 27 August 2023; revised 26 February 2024; accepted 28 February 2024; published 13 March 2024)

The self-energy corrections to phonons have mostly been observed for modes with zone-center ($q = 0$) wave vectors. Here, we investigated the self-energy corrections to phonons in ionic-liquid-gated semiconductors, i.e., monolayer and bilayer WS_2, experimentally. Apart from the previously observed $A_{1g}(\Gamma)$ mode renormalization by Raman spectroscopy, we additionally discovered that the zone-edge longitudinal acoustic (LA(M)) phonon also softened under finite electron doping. This observed renormalization effect arises from the LA(M) phonon-assisted electron scattering between the **K** and **Q** valleys in the conduction bands, indicating the nonadiabatic self-energy corrections dominate, different from the $A_{1g}(\Gamma)$ mode. The self-energy corrections of the two modes both depend on layer configurations. Our findings suggest that WS_2 and other similar two-dimensional materials are intriguing playgrounds to study the electron-phonon interactions and valley-related physics.

DOI: 10.1103/PhysRevB.109.L121202

Electron-phonon interactions (EPIs) are crucial for understanding many important physical phenomena in condensed matter physics. Importantly, EPIs can give self-energy corrections to phonons, responsible for a variety of well-known effects, such as the Kohn anomaly [1–3], Peierls transition [4,5], and other types of phonon renormalizations and perturbations [6–8]. The phonon self-energy corrections have been extensively investigated in metals or narrow gap semiconductors both theoretically and experimentally [4–11]. In the majority of these studies, only the self-energy for the modes with zone-center wave vectors is observed. One of the exceptions is the self-energy corrections to nonzero wave-vector phonons in monolayer graphene, a celebrated two-dimensional (2D) material, arising from phonon-assisted intra- and intervalley scatterings [6,12].

Transition metal dichalcogenides (TMDCs), another kind of 2D material, have garnered significant attention due to their distinctive properties [13–15]. In contrast to graphene, TMDCs possess more energy valleys in the vicinity of the Fermi energy, distributed across different positions of the Brillouin zone. The electron scatterings between different valleys require assistance from momentum-matched phonons. In recent experiments, the detection of spin-forbidden and momentum-forbidden dark excitons in charge-neutral or doped TMDCs suggests a significant intervalley scattering caused by EPIs [16–18]. In doped samples, the energy renormalization of $A_{1g}(\Gamma)$ phonons in TMDCs was observed by a few groups, which was attributed to the adiabatic self-energy corrections due to the screening effect of free carriers within the framework of the Born-Oppenheimer approximation [19–21]. Although the band splitting between **K** (**K**′) and other valleys (**Q** and **Γ**) in TMDCs usually ranges from a few tens of meV to hundreds meV, it is still possible to observe the self-energy corrections to the momentum-matched phonon modes when the energy mismatch is not too large and the EPI is strong.

In this Letter, we focus on WS_2 because the energy splittings between the **K** (**K**′) and **Q** valleys in the conduction bands are small and tunable by layer numbers. By ionic-liquid-gated Raman spectroscopy, $A_{1g}(\Gamma)$ phonons in monolayer WS_2 show an electron doping-dependent softening effect, also reported in previous studies [20]. Importantly, the second-order resonant 2LA(M) longitudinal acoustic mode in monolayer WS_2 is observed to undergo energy renormalization, arising from the LA(M) phonon-assisted electron scattering between the **K** (**K**′) and **Q** valleys [Figs. 1(a) and 1(b)]. In bilayer WS_2, the self-energy correction to the $A_{1g}(\Gamma)$ mode is weakened, while the one to the 2LA(M) mode is still strong, compared to the monolayer scenario. This is due to the direct-to-indirect band-gap transition in bilayer and thicker WS_2. In MoS_2/WS_2 heterostructures, the two modes show a negligible softening effect due to the type-II band alignment. From a unified theoretical analysis, the renormalization of the 2LA(M) phonon is mainly contributed by the nonadiabatic self-energy, different from the one for the $A_{1g}(\Gamma)$ phonon, which is from the screening effect of doped carriers. We discussed alternative material platforms that may yield similar findings.

*luox77@mail.sysu.edu.cn
†yunmeili@xmu.edu.cn

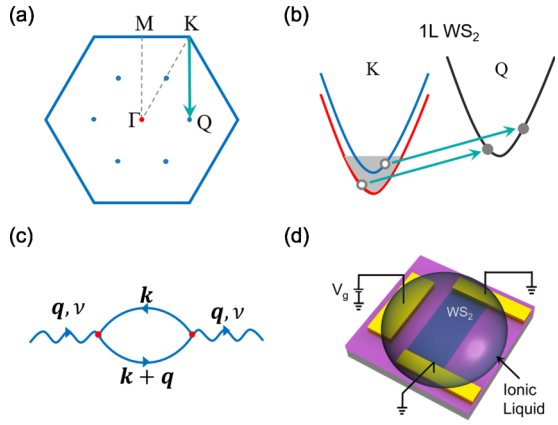

FIG. 1. (a) The first Brillouin zone of monolayer WS_2. The electron transition between **K** and **Q** valleys can be mediated by zone-edge phonons. (b) The illustration of the electron transition from **K** to **Q** valleys in monolayer (1L) WS_2 under electron doping to create electron-hole pairs. (c) The Feynman diagram for electron-phonon self-energy. (d) Schematic device structure for doping WS_2 with electrons by utilizing an ionic liquid as the top gate.

The Feynman diagram for the phonon self-energy due to EPIs is shown in Fig. 1(c). Within the second-order perturbation theory, the phonon self-energy correction can be approximately described as [8,12,22,23]

$$\Pi_{\mathbf{q}\nu} = \frac{1}{N_{\mathbf{k}}} \sum_{\mathbf{k}mn} \frac{\left|V_{mn\nu}^{\mathbf{k},\mathbf{q}}\right|^2 (f_{\mathbf{k},n} - f_{\mathbf{k}+\mathbf{q},m})}{\hbar\omega_{\mathbf{q}\nu} + i\eta_{\mathbf{q}} + \epsilon_{\mathbf{k},n} - \epsilon_{\mathbf{k}+\mathbf{q},m}}, \tag{1}$$

where $V_{mn\nu}^{\mathbf{k},\mathbf{q}}$ is the strength of the EPI, $\epsilon_{\mathbf{k},n}$ is the electron energy of the nth band, and $\omega_{\mathbf{q}\nu}$ is the phonon frequency with ν the phonon mode and $\mathbf{q}$ the phonon wave vector. $\eta_{\mathbf{q}}$ is a small real number, $f_{\mathbf{k},n} = [1 + e^{(\epsilon_{\mathbf{k},n}-\mu)/k_BT}]^{-1}$ is the Fermi-Dirac distribution with μ the Fermi energy. Here, we do not contain a factor of 2 due to the spin splitting of the bands near the Fermi energy of WS_2. The real part of $\Pi_{\mathbf{q}\nu}$ denotes the shift of the phonon energy. $\Delta\omega_{\mathbf{q}\nu} = \omega_{\mathbf{q}\nu} - \omega_{\mathbf{q}\nu}^0 = \mathrm{Re}[\Pi_{\mathbf{q}\nu}]/\hbar$, where $\omega_{\mathbf{q}\nu}^0$ is the phonon frequency in the adiabatic approximation. The decay width is determined by the imaginary part $\mathrm{Im}[\Pi_{\mathbf{q}\nu}]$. The adiabatic self-energy contribution in Eq. (1) is by taking $\omega_{\mathbf{q}\nu} = 0$. The difference between Eq. (1) and the adiabatic contribution is the nonadiabatic self-energy [12,22].

The phonon self-energy correction does not vanish when we have a nonzero EPI strength $V_{mn\nu}^{\mathbf{k},\mathbf{q}}$ and occupied (unoccupied) initial (final) states. The creation of electron-hole pairs by the EPI with an energy difference comparable to the allowed phonon is crucial for the nonzero self-energy. Therefore, doping is essential for the observation of phonon self-energies, given the giant difference between the band gap and phonon energies of WS_2. The doped free carriers in the conduction or valence bands provide the chance to create electron-hole pairs between separated bands and valleys. Although the summation is performed over all the bands and in the whole Brillouin zone, only the combination of electronic states fulfilling the energy and momentum requirements contribute significantly to the phonon self-energy. Notice that the wave vector of **ΓM** is equal to **QK** in the first Brillouin zone, indicating phonon modes with momentum **M** can facilitate

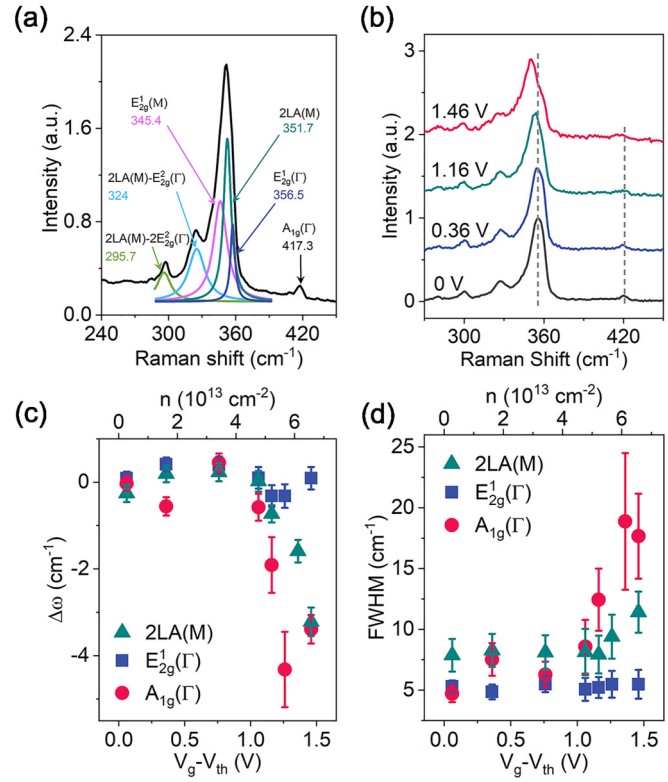

FIG. 2. (a) Raman spectrum of monolayer WS_2. The Raman spectrum peaks are deconvoluted by multipeak Lorentz fitting. The corresponding Raman shift of each peak is labeled alongside. (b) Vertically shifted normalized Raman spectra of monolayer WS_2 at $V_g - V_{\mathrm{th}}$ of 0, 0.36, 1.16, and 1.46 V. The dashed gray lines are visual guides. (c) Shift and (d) FWHM of the 2LA(M) (dark cyan triangles), $E_{2g}^1(\Gamma)$ (blue squares), and $A_{1g}(\Gamma)$ (red circles) Raman modes of monolayer WS_2 as a function of $V_g - V_{\mathrm{th}}$ (bottom axis) or electron density (top axis).

the electron scattering between **K** and **Q** valleys [Figs. 1(a) and 1(b)]. Moreover, the energy difference between the conduction band minimum (CBM) at the **K** and **Q** valleys in monolayer WS_2 is about −50.3 meV according to our first-principles calculations [Sec. S3 of the Supplemental Material (SM) [24]]. These indicate that self-energy corrections are anticipated for the phonon modes at the zone-edge **M** point.

WS_2 monolayers, bilayers, and MoS_2/WS_2 heterostructures were prepared and transferred onto the prefabricated Ti/Au (5 nm/50 nm) electrodes on SiO_2 (300 nm)/Si substrates by a polydimethylsiloxane (PDMS) based dry transfer method (see Sec. S1 of the SM [24] and Refs. [25–29] therein). A droplet of the dehydrated ionic liquid was applied between the sample and the gate electrode as the gate dielectric [see Fig. 1(d)] after being annealed at 250 °C under N_2 gas environment. Raman spectra were measured under 532 nm laser excitation with varying gate voltages. Electron doping density n was estimated by $n = C(V_g - V_{\mathrm{th}})/e$, where V_g and V_{th} are the gate and threshold voltages, respectively. C is capacitance per unit area of the ionic liquid, and e is the unit electron charge.

We focus on monolayer WS_2 first. The Raman spectrum of a charge-neutral monolayer WS_2 is presented in Fig. 2(a). The

phonon mode peaks were deconvoluted by multipeak Lorentz fitting with the Raman shifts labeled. The Raman shifts of the first-order in-plane $E^1_{2g}(\Gamma)$ and out-of-plane $A_{1g}(\Gamma)$ optical phonon modes are observed at 356.5 and 417.3 cm^{-1}, respectively. These values are consistent with previous reports of monolayer WS_2 [30–32]. Another fingerprint of monolayer WS_2 is the second-order resonant 2LA(M) longitudinal acoustic modes at 351.7 cm^{-1} [30]. The separation of Raman shifts between 2LA(M) and $A_{1g}(\Gamma)$ modes is approximately 65.6 cm^{-1}.

Figure 2(b) shows the Raman spectra of monolayer WS_2 under electron doping. By increasing the gate voltage (V_g), the $A_{1g}(\Gamma)$ phonon mode at 417.3 cm^{-1} softens while the $E^1_{2g}(\Gamma)$ mode remains unchanged [Figs. 2(c) and 2(d)], the same as the behaviors of the A_{1g} and E^1_{2g} Raman phonon modes of MoS_2 [19]. The energy of the $A_{1g}(\Gamma)$ phonon is approximately 51.8 meV, significantly larger than the conduction band spin splitting of about 12 meV of the **K** (**K**′) valleys [33]. This far from resonance feature signals that the energy shift is primarily contributed by the adiabatic effect from the doped electrons. The adiabatic self-energy for the $A_{1g}(\Gamma)$ phonon is given by $\Pi^A = \Pi_{\mathbf{q}\to 0,\nu}(\omega = 0)$ [12,22], with

$$\Pi^A = \frac{1}{N_{\mathbf{k}}} \sum_{\mathbf{k}mn} \frac{|V^{\mathbf{k},\mathbf{q}}_{mn\nu}|^2 (f_{\mathbf{k},n} - f_{\mathbf{k}+\mathbf{q},m})}{\epsilon_{\mathbf{k},n} - \epsilon_{\mathbf{k}+\mathbf{q},m}}\Bigg|_{\mathbf{q}\to 0}. \tag{2}$$

The adiabatic self-energy can be divided into two parts: the intraband part and interband one. Here, $\Pi^A = \Pi^A_{\text{intra}} + \Pi^A_{\text{inter}}$. So, $\Pi^A_{\text{intra}} = \frac{1}{N_{\mathbf{k}}} \sum_{\mathbf{k}n} |V^{\mathbf{k},\mathbf{q}=0}_{nn\nu}|^2 \frac{\partial f_{\mathbf{k},n}}{\partial \epsilon_{\mathbf{k},n}} \simeq -n(\mu)\overline{g^2(\mu)}$ at low temperatures. $n(\mu)$ is the density of states at the Fermi energy. $g^2(\mu) = |V^{\mathbf{k},\mathbf{q}=0}_{nn\nu}|^2$ and $\overline{g^2(\mu)}$ is the average around the Fermi level. The interband transition Π^A_{inter} is the result in Eq. (2) when $m \neq n$. The results of the doping-dependent shifts of the $A_{1g}(\Gamma)$ and $E^1_{2g}(\Gamma)$ modes based on first-principle calculations are presented in Sec. S5 of the SM [24], showing good agreement with our experimental observations. The change in the frequency shift and full width at half maximum (FWHM) around $V_g - V_{\text{th}} = 1.25$ V for the $A_{1g}(\Gamma)$ mode in Figs. 2(c) and 2(d) is probably due to the filling effect. The population of **Q** valleys above this gate voltage changes the Fermi surface.

The second-order resonant 2LA(M) mode dominates the Raman spectrum of monolayer WS_2. The increasing gate voltage V_g softens the phonon energy and broadens the linewidth, as shown in Fig. 2(b). At $V_g - V_{\text{th}} = 1.46$ V, the frequency reduces by a wave number 3.22 cm^{-1} while the FWHM broadens by 3.50 cm^{-1} [Figs. 2(c) and 2(d)]. As discussed above, the LA(M) phonon facilitates the electron transition between the **K** and **Q** valleys by compensating the intervalley momentum mismatch. In addition, the energy of the 2LA(M) mode (about 43.6 meV) is comparable to the calculated energy difference between the **K** (**K**′) and **Q** valleys (about −50.3 meV), while the spin splitting at the **K** (**K**′) valleys is only about 12 meV. Therefore, the energy difference between **K** (**K**′) and **Q** valleys is comparable to the energy of the LA(M) phonon. The in close resonance condition suggests that the nonadiabatic self-energy dominates. From a qualitative analysis, the absolute value of the denominator $|\hbar\omega_{\mathbf{q}\nu} + \epsilon_{\mathbf{k},n} - \epsilon_{\mathbf{k}+\mathbf{q},m}|$ is much smaller than the one of the adiabatic part $|\epsilon_{\mathbf{k},n} - \epsilon_{\mathbf{k}+\mathbf{q},m}|$. This analysis yields

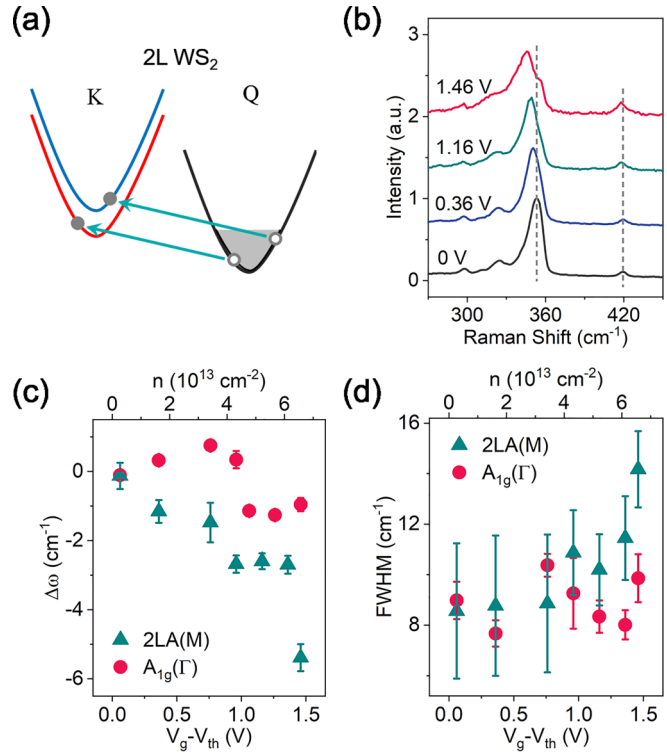

FIG. 3. (a) A depiction of the electron transition from the **Q** to **K** valleys in bilayer (2L) WS_2 when subjected to electron doping. (b) Normalized Raman spectra of bilayer WS_2 at $V_g - V_{\text{th}}$ of 0, 0.36, 1.16, and 1.46 V. Raman spectra were shifted vertically for comparison. The dashed gray lines serve as visual guides. The variation of (c) shift and (d) FWHM of the 2LA(M) (dark cyan triangles) and $A_{1g}(\Gamma)$ (red circles) Raman modes of bilayer WS_2 with respect to $V_g - V_{\text{th}}$ (bottom axis) or electron density (top axis).

a negative real value of the self-energy, consistent with our experimental observations. Here, we should emphasize that the multivalley band structures are vital for the observation of self-energy corrections to nonzero wave-vector phonons. Typically, the multiple valleys appearing in the bands are determined by symmetry constraints and commonly locate at high-symmetry points or lines. The electronic intervalley scatterings require a momentum compensation from phonons on the high-symmetric points or lines, some of which can be detected by Raman techniques.

There is a direct-to-indirect transition in the band structures when the layer number is increased for WS_2 from the first-principles calculations [24]. The energy of the **Q** valleys for few-layer and bulk WS_2 is smaller than that of the **K** (**K**′) valleys in the conduction bands, as illustrated in Fig. 3(a). When free electrons are doped, the **Q** valleys will be populated first, different from the monolayer case. We here discuss only the bilayer case as thicker ones are expected to exhibit the same behavior. The Raman spectra at four different gate voltages are presented in Fig. 3(b). The deconvoluted spectra are presented in Sec. S6 of the SM [24]. The gate voltage-dependent Raman shift and line broadening of the $A_{1g}(\Gamma)$ and 2LA(M) modes are displayed in Figs. 3(c) and 3(d), respectively. We can see that the $A_{1g}(\Gamma)$ mode shows a much weaker dependence on electrostatic dopings

compared to the monolayer case. As the self-energy of the $A_{1g}(\Gamma)$ phonon is mainly determined by the Fermi surface properties, the different population in bilayer WS_2 leads to distinct Fermi-surface properties, resulting in a less pronounced effect.

By contrast, the 2LA(M) mode still exhibits a strong gate voltage dependence, as shown in Fig. 3(c). When $V_g - V_{\text{th}}$ is increased from 0 to 1.46 V, the wave number of the 2LA(M) mode redshifts by 5.40 cm^{-1} and FWHM broadens by 6.43 cm^{-1}, even a little larger than that observed in the monolayer counterpart. Although the population is different in the bilayer samples, the 2LA(M) phonon can still facilitate the electron transitions between the **K** (**K**′) and **Q** valleys, as depicted in Fig. 3(a). The only difference is the reversed scattering path. The strong EPIs ($V_{mnv}^{\mathbf{k},\mathbf{q}}$) still renormalize the 2LA(M) phonon, even resulting in a more pronounced effect. Similarly, the change in the frequency shift around $V_g - V_{\text{th}} = 1.25$ V for the 2LA(M) and $A_{1g}(\Gamma)$ modes could be possibly attributed to the simultaneous population of the valleys and the split bands.

We further examine the scenario of MoS_2/WS_2 heterostructures (MoS_2 on top of WS_2) to gain additional insight into the aforementioned findings. MoS_2/WS_2 heterostructures have a type-II band alignment, where the energy of the **K** (**K**′) valleys in MoS_2 is much lower than that of WS_2, as illustrated in Fig. 4(a). Most of the doped electrons fill the conduction band of the MoS_2 layer, while the bands in the WS_2 layer remain almost unoccupied. As a consequence, the peaks of the 2LA(M) and $A_{1g}(\Gamma)$ phonons of WS_2 in the Raman spectra show a considerably weaker dependence on the gate voltage, as displayed in Figs. 4(b) and 4(c). The deconvoluted spectra of WS_2 in the heterostructures are displayed in Sec. S7 of the SM [24]. Even at a high electron doping density, the frequency shifts are quite small. Similar results were obtained for the heterostructures with WS_2 stacking on top of MoS_2. Both the 2LA(M) and $A_{1g}(\Gamma)$ phonon modes still remain largely unaffected even under high electron doping levels. Most of the electrons still occupy the **K** valley of MoS_2, independent on the stacking sequence. The detailed analysis is in Sec. S9 of the SM [24].

As most of the doped electrons occupy the conduction bands of MoS_2 in the heterostructure, the free carriers are expected to renormalize the phonon energy of MoS_2. In Fig. 4(d), we present the energy shifts of the $E_{2g}^1(\Gamma)$ and $A_{1g}(\Gamma)$ phonons of MoS_2. Similar to monolayer WS_2, the $E_{2g}^1(\Gamma)$ mode of MoS_2 is insensitive to electron doping, while the $A_{1g}(\Gamma)$ mode shows a doping-dependent redshift. The underlying mechanism is the same as that of WS_2, i.e., the adiabatic effect from the doped electrons. Bilayer MoS_2 also exhibits a similar behavior, with the results presented in Sec. S11 of the SM [24].

Here, the 2LA(M) mode of MoS_2 is not observed in the Raman spectrum because of the larger energy difference between the **K** and **Q** valleys. The deviation from resonance indicates a negligible weak self-energy correction. The Raman spectrum of monolayer WSe_2 shows a weaker 2LA(M) signal compared to WS_2 [20]. The energy renormalization of the 2LA(M) phonon in doped WSe_2 is also expected. The Janus material WSSe shows a small energy difference between the **K** (**K**′) and **Q** valleys [34], presaging another promising platform to observe similar results.

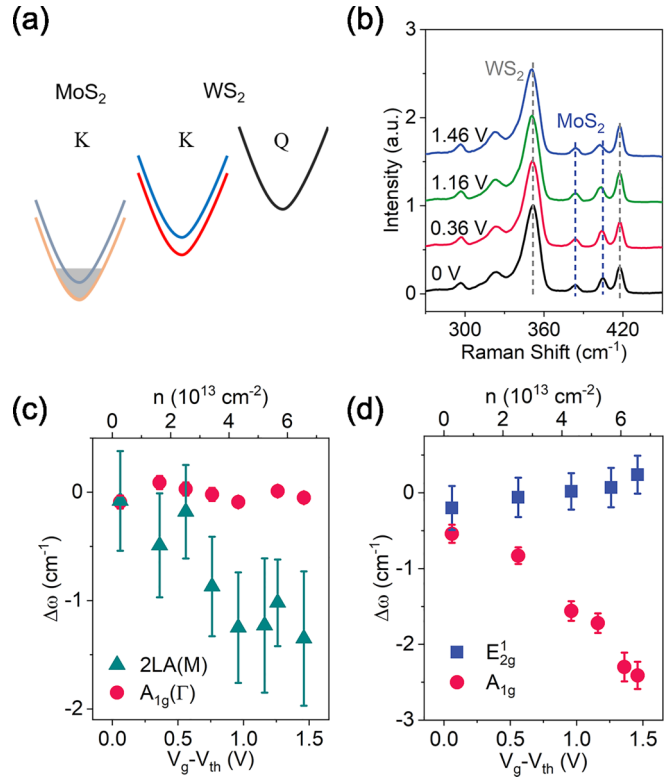

FIG. 4. (a) The schematic band structure of MoS_2/WS_2 heterostructures when under electron doping. Electrons were primarily doped to the **K** valley of MoS_2. (b) Vertically shifted normalized Raman spectra of MoS_2/WS_2 heterostructures when $V_g - V_{\text{th}}$ equals 0, 0.36, 1.16, and 1.46 V. The gray (WS_2) and blue (MoS_2) dashed lines are visual guides. Shift of the 2LA(M) (dark cyan triangles) and $A_{1g}(\Gamma)$ (red circles) Raman modes of WS_2 (c) and E_{2g}^1 (blue squares), and A_{1g} (red circles) Raman modes of MoS_2 in the heterostructure as a function of $V_g - V_{\text{th}}$ (bottom axis) or electron density (top axis).

In summary, we investigated the phonon energy renormalization in monolayer WS_2, bilayer WS_2, and MoS_2/WS_2 heterostructures by ionic-liquid-gated Raman spectroscopy under electron doping. Owing to the intervalley scatterings mediated by EPIs, the phonon mode 2LA(M) was observed to acquire doping-dependent self-energy corrections, dominated by the nonadiabatic contribution, different from the mechanism for the observed zone-center $A_{1g}(\Gamma)$ mode. The self-energy corrections of both modes were dependent on the layer constitutions, arising from the band engineering in the bilayer structures. We also discussed that other materials such as WSe_2 and WSSe were also expected to show similar results considering the near resonance energy of the 2LA(M) phonon and the energy difference between the **K** and **Q** valleys.

Q.W. and Y.-M.L. acknowledge the support from Xiamen University. Q.W. acknowledges financial support from the National Natural Science Foundation of China (Grant No. 62304186). Y.-M.L. acknowledges the support from the MOST of China with Grant No. 2022YFA1204700. X.L. acknowledges the support from the NSFC (Grant No. 12172386), the National Natural Science Foundation of Guangdong Province (Grant No. 2021B1515020021),

and the Guangdong Provincial Key Laboratory of Magnetoelectric Physics and Devices (LaMPad) (Grant No. 2022B1212010008). Y.L.H. acknowledges the support from NSFC (Grant No. 12004278) and the Natural Science Foundation of Fujian Province (Grant No. 2022J06035). Q.Z. acknowledges the National Natural Science Foundation of China (Grant No. 12304465) and the Natural Science Foundation of Jiangsu Province (Grant No. BK20230831).

[1] W. Kohn, Image of the Fermi surface in the vibration spectrum of a metal, Phys. Rev. Lett. **2**, 393 (1959).
[2] S. Piscanec, M. Lazzeri, F. Mauri, A. C. Ferrari, and J. Robertson, Kohn anomalies and electron-phonon interactions in graphite, Phys. Rev. Lett. **93**, 185503 (2004).
[3] M. Lazzeri and F. Mauri, Nonadiabatic Kohn anomaly in a doped graphene monolayer, Phys. Rev. Lett. **97**, 266407 (2006).
[4] A. Sédéki, L. G. Caron, and C. Bourbonnais, Electron-phonon coupling and Peierls transition in metallic carbon nanotubes, Phys. Rev. B **62**, 6975 (2000).
[5] O. Dubay, G. Kresse, and H. Kuzmany, Phonon softening in metallic nanotubes by a Peierls-like mechanism, Phys. Rev. Lett. **88**, 235506 (2002).
[6] D. L. Mafra, J. Kong, K. Sato, R. Saito, M. S. Dresselhaus, and P. T. Araujo, Using gate-modulated Raman scattering and electron-phonon interactions to probe single-layer graphene: A different approach to assign phonon combination modes, Phys. Rev. B **86**, 195434 (2012).
[7] H. Farhat, K. Sasaki, M. Kalbac, M. Hofmann, R. Saito, M. S. Dresselhaus, and J. Kong, Softening of the radial breathing mode in metallic carbon nanotubes, Phys. Rev. Lett. **102**, 126804 (2009).
[8] A. H. Castro Neto, F. Guinea, N. M. R. Peres, K. S. Novoselov, and A. K. Geim, The electronic properties of graphene, Rev. Mod. Phys. **81**, 109 (2009).
[9] A. Marco Saitta, M. Lazzeri, M. Calandra, and F. Mauri, Giant nonadiabatic effects in layer metals: Raman spectra of intercalated graphite explained, Phys. Rev. Lett. **100**, 226401 (2008).
[10] N. Caudal, A. Marco Saitta, M. Lazzeri, and F. Mauri, Kohn anomalies and nonadiabaticity in doped carbon nanotubes, Phys. Rev. B **75**, 115423 (2007).
[11] J. Hlinka, I. Gregora, J. Pokorny, C. Hérold, N. Emery, J. F. Marêché, and P. Lagrange, Lattice dynamics of CaC_6 by Raman spectroscopy, Phys. Rev. B **76**, 144512 (2007).
[12] P. T. Araujo, D. L. Mafra, K. Sato, R. Saito, J. Kong, and M. S. Dresselhaus, Phonon self-energy corrections to nonzero wavevector phonon modes in single-layer graphene, Phys. Rev. Lett. **109**, 046801 (2012).
[13] D. Xiao, G.-B. Liu, W. Feng, X. Xu, and W. Yao, Coupled spin and valley physics in monolayers of MoS_2 and other group-VI dichalcogenides, Phys. Rev. Lett. **108**, 196802 (2012).
[14] Q. H. Wang, K. Kalantar-Zadeh, A. Kis, J. N. Coleman, and M. S. Strano, Electronics and optoelectronics of two-dimensional transition metal dichalcogenides, Nat. Nanotechnol. **7**, 699 (2012).
[15] D. M. Kennes, M. Claassen, L. Xian, A. Georges, A. J. Millis, J. Hone, C. R. Dean, D. N. Basov, A. N. Pasupathy, and A. Rubio, Moiré heterostructures as a condensed-matter quantum simulator, Nat. Phys. **17**, 155 (2021).
[16] Z. Li, T. Wang, S. Miao, Y. Li, Z. Lu, C. Jin, Z. Lian, Y. Meng, M. Blei, T. Taniguchi, K. Watanabe, S. Tongay, W. Yao, D. Smirnov, C. Zhang, and S.-F. Shi, Phonon-exciton interactions in WSe_2 under a quantizing magnetic field, Nat. Commun. **11**, 3104 (2020).
[17] J. Madéo, M. K. L. Man, C. Sahoo, M. Campbell, V. Pareek, E. L. Wong, A. Al-Mahboob, Nicholas S. Chan, Arka Karmakar, B. M. K. Mariserla, X. Li, T. F. Heinz, T. Cao, and K. M. Dani, Directly visualizing the momentum-forbidden dark excitons and their dynamics in atomically thin semiconductors, Science **370**, 1199 (2020).
[18] Q.-H. Tan, Y.-M. Li, J.-M. Lai, Y.-J. Sun, Z. Zhang, F. Song, C. Robert, X. Marie, W. Gao, P.-H. Tan, and J. Zhang, Quantum interference between dark-excitons and zone-edged acoustic phonons in few-layer WS_2, Nat. Commun. **14**, 88 (2023).
[19] B. Chakraborty, A. Bera, D. V. S. Muthu, S. Bhowmick, U. V. Waghmare, and A. K. Sood, Symmetry-dependent phonon renormalization in monolayer MoS_2 transistor, Phys. Rev. B **85**, 161403(R) (2012).
[20] T. Sohier, E. Ponomarev, M. Gibertini, H. Berger, N. Marzari, N. Ubrig, and A. F. Morpurgo, Enhanced electron-phonon interaction in multivalley materials, Phys. Rev. X **9**, 031019 (2019).
[21] M. W. Iqbal, K. Shahzad, G. Hussain, M. K. Arshad, R. Akbar, S. Azam, S. Aftab, T. Alharbi, and A. Majid, Gate dependent phonon shift in tungsten disulfide (WS_2) field effect transistor, Mater. Res. Express **6**, 115909 (2019).
[22] F. Giustino, Electron-phonon interactions from first principles, Rev. Mod. Phys. **89**, 015003 (2017).
[23] M. Calandra, G. Profeta, and F. Mauri, Adiabatic and nonadiabatic phonon dispersion in a Wannier function approach, Phys. Rev. B **82**, 165111 (2010).
[24] See Supplemental Material at http://link.aps.org/supplemental/10.1103/PhysRevB.109.L121202 for details of our experimental data, which includes Refs. [25–29].
[25] Q. Wang and A. T. S. Wee, Upconversion photovoltaic effect of WS_2/2D perovskite heterostructures by two-photon absorption, ACS Nano **15**, 10437 (2021).
[26] Q. Wang, J. Maisch, F. Tang, D. Zhao, S. Yang, R. Joos, S. L. Portalupi, P. Michler, and J. H. Smet, Highly polarized single photons from strain-induced quasi-1D localized excitons in WSe_2, Nano Lett. **21**, 7175 (2021).
[27] J. Ye, S. Inoue, K. Kobayashi, Y. Kasahara, H. Yuan, H. Shimotani, and Y. Iwasa, Liquid-gated interface superconductivity on an atomically flat film, Nat. Mater. **9**, 125 (2010).
[28] Y. Zhang, J. Ye, Y. Matsuhashi, and Y. Iwasa, Ambipolar MoS_2 thin flake transistors, Nano Lett. **12**, 1136 (2012).
[29] Y. Wang, J. Xiao, H. Zhu, Y. Li, Y. Alsaid, K. Yan Fong, Y. Zhou, S. Wang, W. Shi, Y. Wang, A. Zettl, E. J. Reed, and X. Zhang, Structural phase transition in monolayer $MoTe_2$ driven by electrostatic doping, Nature (London) **550**, 487 (2017).
[30] M. W. Iqbal, M. Z. Iqbal, M. F. Khan, M. A. Shehzad, Y. Seo, J. H. Park, C. Hwang, and J. Eom, High-mobility and air-stable single-layer WS_2 field-effect transistors sandwiched

between chemical vapor deposition-grown hexagonal BN films, Sci. Rep. **5**, 10699 (2015).

[31] C. Cong, J. Shang, X. Wu, B. Cao, N. Peimyoo, C. Qiu, L. Sun, and T. Yu, Synthesis and optical properties of large-area single-crystalline 2D semiconductor WS_2 monolayer from chemical vapor deposition, Adv. Opt. Mater. **2**, 131 (2014).

[32] H. R. Gutiérrez, N. Perea-López, A. L. Elías, A. Berkdemir, B. Wang, R. Lv, F. López-Urías, V. H. Crespi, H. Terrones, and M. Terrones, Extraordinary room-temperature photoluminescence in triangular WS_2 monolayers, Nano Lett. **13**, 3447 (2013).

[33] L. Ren, C. Robert, H. Dery, M. He, P. Li, D. V. Tuan, P. Renucci, D. Lagarde, T. Taniguchi, K. Watanabe, X. Xu, and X. Marie, Measurement of the conduction band spin-orbit splitting in WSe_2 and WS_2 monolayers, Phys. Rev. B **107**, 245407 (2023).

[34] S.-B. Yu, S.-H. Sun, M. Zhou, D. Zhang, and K. Chang, Current-induced spin polarization in Janus WSSe monolayer, Phys. Rev. B **107**, 125426 (2023).